Enhancement of CO_2 Adsorption and CO_2/N_2 Selectivity on ZIF-8 via Postsynthetic Modification

Zhijuan Zhang
School of Chemistry and Chemical Engineering, South China University of Technology, Guangzhou, 510640, P.R. China

Dept. of Chemistry and Chemical Biology, Rutgers University, Piscataway, New Jersey, 08854

Shikai Xian, Qibin Xia, Haihui Wang, and Zhong Li
School of Chemistry and Chemical Engineering, South China University of Technology, Guangzhou, 510640, P.R. China

Jing Li
Dept. of Chemistry and Chemical Biology, Rutgers University, Piscataway, New Jersey, 08854

DOI 10.1002/aic.13970
Published online January 11, 2013 in Wiley Online Library (wileyonlinelibrary.com)

Imidazolate framework ZIF-8 is modified via postsynthetic method using etheylenediamine to improve its adsorption performance toward CO_2. Results show that the BET surface area of the modified ZIF-8 (ED-ZIF-8) increases by 39%, and its adsorption capacity of CO_2 per surface area is almost two times of that on ZIF-8 at 298 K and 25 bar. H_2O uptake on the ED-ZIF-8 become obviously lower compared to the ZIF-8. The ED-ZIF-8 selectivity for CO_2/N_2 adsorption gets significantly improved, and is up to 23 and 13.9 separately at 0.1 and 0.5 bar, being almost twice of those of the ZIF-8. The isosteric heat of CO_2 adsorption (Q_{st}) on the ED-ZIF-8 becomes higher, while Q_{st} of N_2 gets slightly lower compared to those on the ZIF-8 Furthermore, it suggests that the postsynthetic modification of the ZIF-8 not only improves its adsorption capacity of CO_2 greatly, but also enhances its adsorption selectivity for $CO_2/N_2/H_2O$ significantly.
 AIChE J, 59: 2195–2206, 2013
Keywords: ZIF-8, modification, adsorption/gas, isosteric heat of adsorption, selectivity

Introduction

CO_2 has often been cited as the primary anthropogenic greenhouse gas (GHG) as well as the leading culprit in global climate change. The development of a viable carbon capture and sequestration technology (CCS), is therefore, a scientific challenge of the highest order.[1–4] Currently, a variety of methods, such as membrane separation, chemical absorption with solvents, and adsorption with solid adsorbents, have been proposed to sequester CO_2 from the flue gases of power plant. Thereinto, the adsorption is considered to be one of the most promising technologies for capturing CO_2 from flue gases because of their easy control, low operating and capital costs, and superior energy efficiency.[5–7] Many adsorbents have been investigated for CO_2 adsorption including activated carbons, zeolites, hydrotalcites and metal oxides.[8–14] However, although some zeolite materials have been claimed to be most adequate for CO_2 separation from flue streams, it is difficult to regenerate them without significant heating which leads to low productivity and great expense.[15,16]

Recently, metal-organic frameworks (MOFs) have attracted great attention and present a promising platform for the development of next-generation capture materials because of their high capacity for gas adsorption and tunable pore surfaces that can facilitate highly selective binding of CO_2.[17–26] To optimize a MOF for a particular application, it is important to be able to tailor its pore metrics and functionality in a straightforward fashion. However, tailoring MOFs materials by modifying their textural properties (e.g., surface area and pore volume) and surface chemistry (acid–base properties, functional groups) for adsorption application is still a difficult task.[27] Many researchers have given insight into modification of the MOF materials so as to develop new and better adsorbents. Strategies reported include ligand functionalization,[24,28–39] framework interpenetration,[22,23] introduction of alkali-metal cations,[40–42] control of pore size[32,43–47] and incorporation of open metal sites (OMSs).[39,48–51] However, because of the instability under conditions for the synthesis of MOFs or the competitive reaction with some framework components, it may be difficult for certain functional groups to incorporate into MOFs using aforementioned strategies. Another strategy for generating desired functionalities in MOFs is the postsynthesis

Additional Supporting Information may be found in the online version of this article.

Correspondence concerning this article should be addressed to Z. Li at cezhli@scut.edu.cn.

modification of preconstructed, robust precursor MOFs.[52–55] For example, An et al.[33] demonstrated that postsynthetic exchange of extra-framework cations within anionic bio-MOF-1[56] can be used as a means to systematically modify its pore dimensions and metrics. Farha et al.[57] synthesized a series of cavity modified MOFs by replacing coordinated solvents with several different pyridine ligands. They found that a p-$(CF_3)NC_5H_4$-modified MOF showed considerable improvements in the CO_2/N_2 selectivities compared to the parent framework.[46] Long and his coworkers[58] previously reported the grafting of ethylenediamine (en) within a water-stable MOF $H_3[(Cu_4Cl)_3(BTTri)_8]$ (CuBTTri), and found that the en modified sample had more greater attraction of CO_2 at low pressures and the CO_2/N_2 selectivity also increased over the entire pressure range measured. More recently, Long and coworkers[59] incorporated the *N,N′*-dimethylethylenediamine (mmen) into the CuBTTri MOF, and showed that the CO_2 uptake was drastically enhanced. Zhang et al.[60] reported that after ZIF-8 was modified by ammonia impregnation, the surface basicity was greatly increased and therefore the CO_2 uptake was enhanced. Park et al.[61] reported a postsynthetic reversible incorporation of organic linkers 3,6-di(4-pyridyl)-1,2,4,5-tetrazine (bpta) into SNU-30 $[Zn_2(TCPBDA)(H_2O)_2]\cdot 30DMF\cdot 6H_2O$ through single-crystal-to-single-crystal transformations, and found that the desolvated SNU-31′ exhibited enhanced selective adsorption of CO_2 over N_2. Xiang et al.[62] incorporated the CNTs into HKUST-1, and then modified it with Li^+. The results showed that the hybrid Li@CNT@$[Cu_3(btc)_2]$, which is formed by the combination of Li doping and CNT incorporation, having an enhancement of CO_2 uptakes by about 305%. However, to this date, no work has been reported out on the postsynthetic modification of ZIF-8 to enhance its functionality.

In this work, the postsynthetic modification of the ZIF-8 is proposed to prepare a novel adsorbent with higher CO_2 adsorption capacity and CO_2/N_2 selectivity. The postsynthetic modification of the ZIF-8 crystals would be carried out by using ethylenediamine treatment. Then the surface groups of the modified ZIF-8 samples (ED-ZIF-8) would be characterized. Single-component isotherms of CO_2 and N_2 on the modified ZIF-8 samples would be measured separately. Furthermore, the CO_2/N_2 selectivity is estimated by using IAST on the basis of single-component isotherms of CO_2 and N_2. The influence of the textural structures and surface chemistry of the original and modified ZIF-8 samples on their adsorption capacities for CO_2 and selectivity of CO_2/N_2 would be discussed and reported here. This information will be valuable for selecting appropriate adsorbents for CO_2 capture process.

Methods and Materials

Materials and instruments

Zinc nitrate hexahydrate ($Zn(NO_3)_2\cdot 6H_2O$, 98%, extra purity) and 2-methylimidazole (H—MeIM) (99% purity) were purchased from J & K Chemicals. *N,N*— Dimethylacetamide (DMF) was purchased from Qiangshen Chemicals Co., Ltd. of Jiangshu (Jiangshu, China), and it was further purified by 4A molecular sieve to eliminate the water.

Maganetic suspension balance RUBOTHERM was supplied by Germany. Its precision was 0.000001 g. ASAP 2010 sorptometer was supplied by Micromeritics Co., Norcross, GA, USA.

Adsorbents

Synthesis of ZIF-8 was performed following the reported procedures[63] with a few modifications. First, a solid mixture of zinc nitrate hexahydrate $Zn(NO_3)_2\cdot 6H_2O$ (0.956 g, 3.2 mmol) and 2-methylimidazole (H—MeIM) (0.24 g, 3.4 mmol) was dissolved in 70 mL of DMF solvent. The mixture was quickly transferred to a 100 mL autoclave and sealed. Second, the autoclave was heated at a rate of 5 K/min to 413 K in a programmable oven and held at this temperature for 24 h under autogenous pressure by solvothermal synthesis, followed by cooling at a rate of 0.3 K/min to room temperature. Third, after removal of mother liquor from the mixture, chloroform (40 mL) was added to the autoclave. The as-synthesized ZIF-8 crystals were then isolated by filtration. Colorless polyhedral crystals were collected from the upper layer, washed with DMF (10 mL × 3), and dried at 383 K overnight.

To further remove the guest species from the framework and prepare the evacuated form of ZIF-8 crystals for modification and gas-sorption analysis, the as-synthesized ZIF samples were immersed in methanol at ambient temperature for 48 h, and evacuated at ambient temperature for 5 h, and subsequently at an elevated temperature 673 K for 2 h.

Postsynthetic modification of adsorbents

The as-synthesized ZIF-8 crystals (labeled as ZIF-8) were dried at 383 K for 24 h for postsynthetic modification.

The subsequent treatment applied to the modification of ZIF-8 crystals consists of the following steps: The modified ZIF-8 sample (labeled as ED-ZIF-8) was synthesized using ethylenediamine as a linker. In a typical procedure, the ZIF-8 sample was added to 30% ethylenediamine solution and then the mixture was placed in a stainless high-pressure autoclave. The autoclave was heated in an oven at 416 K for 1 h and then 381 K for 6 h. The light yellow product was filtered and washed with deionized water. Finally, the sample was dried at 383 K overnight.

Characterization of adsorbents

The specific surface area and pore volume of original ZIF-8 and modified ZIF-8 crystals were measured on a Micrometrics gas adsorption analyzer ASAP 2010 instrument equipped with commercial software for calculation and analysis.

Powder X-ray diffraction data were collected using a D8 advance θ-2θ diffractometer (Bruker) in reflectance Bragg-Brentano geometry employing Cu Kα line focused radiation with 40 kV voltages and 40 mA current. The X-ray scanning speed was set at 2°/min and a step size of 0.02° in 2θ. A Jade 5 XRD pattern processing software (MDI, Inc., Livermore, CA) was used to analyze the XRD data collected on the ZIF-8 samples.

The surface organic molecules were analyzed by taking FTIR spectra on a Bruker 550 FTIR instrument equipped with a diffuse reflectance accessory that included a reaction cell. Data acquisition was performed automatically using an interfaced computer and a standard software package. The samples were dried *in vacuo* at 423 K prior to mixing with KBr powder. The samples were run in ratio mode allowing for subtraction of a pure KBr baseline. The sample chamber

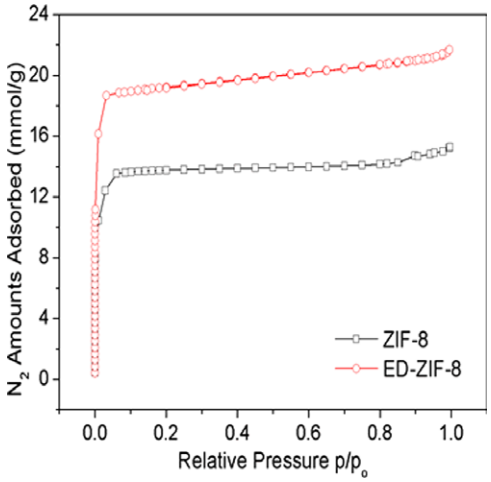

Figure 1. N_2 adsorption-desorption isotherms of ZIF-8 and ED-ZIF-8 samples.

[Color figure can be viewed in the online issue, which is available at wileyonlinelibrary.com.]

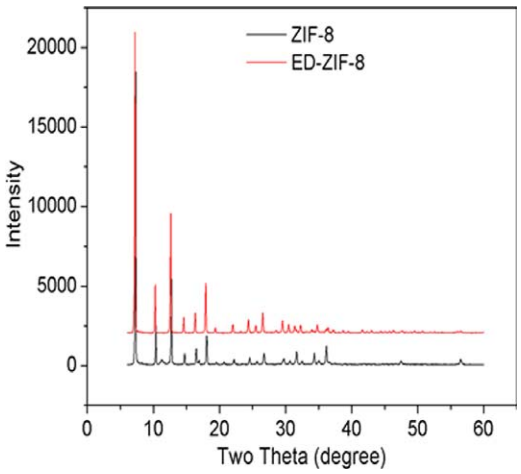

Figure 2. PXRD patterns of ZIF-8 and ED-ZIF-8 samples.

[Color figure can be viewed in the online issue, which is available at wileyonlinelibrary.com.]

was kept purged with nitrogen during the entire experiment. The spectrometer collected 64 spectra in the range of 400–4,000 cm^{-1}, with a resolution of 4 cm^{-1}.

CO_2 and N_2 adsorption measurements

The CO_2 and N_2 adsorption-desorption isotherms at 298 K, 308 K, 318 K, and 328 K were obtained on a RUBOTHERM magnetic suspension balance. The initial activation of the modified sample was carried out at 423 K for 12 h in a vacuum environment. He (ultra-high purity, U-sung) was used as a purge gas in this study. The adsorption processes were carried out using high purity CO_2 and N_2 (99.999%) gas. A feed flow rate of 60 mL/min of CO_2, 40 mL/min of N_2 and 30 mL/min of He, respectively, were controlled with the mass flow controllers (MFC) to the sample chamber. Both adsorption and desorption experiments were conducted at the same temperature. The temperature of the sorption chamber can be adjusted and maintained constant by an internal temperature sensor. However, the pressure can be changed stepwise through the gas flow rate.

Typically, there are four steps for finishing determination of an isotherm of CO_2 or N_2 by using Rubotherm magnetic suspension balance. These detail steps are shown by the operation manual of Rubotherm maganetic suspension balance.

H_2O adsorption measurements

The water adsorption measurements were conducted on a computer-controlled DuPont Model 990 TGA. The partial pressure of water was varied by changing the blending ratios of water-saturated nitrogen and pure nitrogen gas streams. Before measurement, the modified ZIF-8 samples were activated at 423 K for 6 h.

Results and Discussion

Structure and pore characterization

Figure 1 exhibits the adsorption-desorption isotherms of N_2 at 77 K on the two samples ZIF-8 and ED-ZIF-8. It can be seen that both samples show type-I behavior, indicating they are microporous in nature. Table 1 lists structure parameters of the two samples. These data indicate that the BET surface area and micropore volume of the ED-ZIF-8 sample are significantly higher than those of the original ZIF-8 sample, with an increase of ~39% and 35.6%, respectively. Yaghi and his coworkers reported a pore volume of 0.66 cm^3/g for ZIF-8 from the single crystal structure. For the ZIF-8 sample, the total pore volume is calculated to be 0.54 cm^3/g, because part of the pores might be blocked. However, after the postsynthetic modification, the blocked pores were reopened, and at meanwhile, some new pores were formed.[64,65] Thus, the total pore volume of the ED-ZIF-8 sample is greatly improved.

Figure 2 shows the powder X-ray diffraction (PXRD) pattern of the modified ZIF-8 sample. It can be seen that the main peaks of the modified ZIF-8 sample are very clear, and similar to those of the original ZIF-8 sample, indicating that the integrity of the modified ZIF-8 sample maintains well after the postsynthetic modification. However, for a deep looking, it can be found that the major peaks of ED-ZIF-8 all shifted to the left side (low-angle area) a little bit, which means after modification, the lattice distance increased.

In order to obtain information concerning changes in the surface groups, FTIR experiments were carried out to characterize the samples. Figure 3a shows the FTIR spectra of the original ZIF-8 and the ED-ZIF-8 sample. It is noticed that the spectra for the two samples show high similarities, and the main peaks of both ZIF-8 samples match well with the published FTIR spectra for the ZIF-8. However, some

Table 1. Porous Structure Parameters of the Modified ZIF-8 Crystals

Sample	BET surface area ($m^2.g^{-1}$)	Langmuir surface area ($m^2.g^{-1}$)	Micropore volume ($cm^3.g^{-1}$)	Total pore volume ($cm^3.g^{-1}$)	Micropore diameter (nm)	Mesopore diameter (nm)
ZIF-8	1025	1352	0.45	0.54	0.352	4.43
ED-ZIF-8	1428	1897	0.61	0.75	0.544	4.53

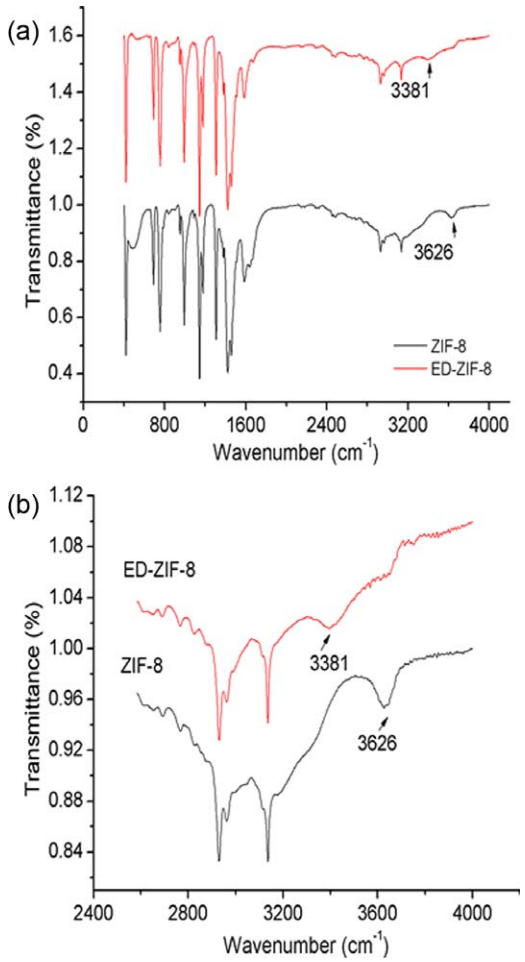

Figure 3. a. FTIR spectra of the modified ZIF-8 crystals between 4,000–400 cm^{-1}; b. FTIR spectra of the modified ZIF-8 crystals between 4000–2,400 cm^{-1}.

[Color figure can be viewed in the online issue, which is available at wileyonlinelibrary.com.]

differences are also observed. For example, the spectrum of the ED-ZIF-8 sample is different from that of the ZIF-8 sample in that (1) as shown in Figure 3b there is a new peak at 3381 cm^{-1} which is assigned to N—H group appeared on the spectrum of the ED-ZIF-8 sample, suggesting some N—H groups have been introduced on the surfaces of the sample ED-ZIF-8, and (2) a peak at 3626 cm^{-1} assigned to O—H of the adsorbed H_2O is present in the spectrum of the ZIF-8 sample, which is absent in the spectrum of the ED-ZIF-8 sample, as shown in Figure 3b.

CO_2 and N_2 adsorption isotherms

For comparison, Figure 4 shows the isotherms of CO_2 on the ZIF-8 and ED-ZIF-8 samples. It is visible that the amount adsorbed of CO_2 increases as temperature decreases. This suggests that the adsorption of CO_2 is mainly physical adsorption. More importantly, it is found that the ED-ZIF-8 sample had higher CO_2 adsorption capacities compared to the ZIF-8 sample, indicating that the adsorption capacities of the modified ZIF-8 toward CO_2 are greatly improved, nearly being twice as much as the ZIF-8. One of the reasons is that the surface area (BET) of the ED-ZIF-8 increases by 39%, as indicated in Table 1. The other reason is that adsorption capacity per unit surface area of the ED-ZIF-8 for CO_2 increases due to an introduction of N—H groups by postsynthetic modification. To further understand that, Figure 4a and 4b are separately transferred into Figure 5a and 5b in which the equilibrium uptakes of CO_2 based on unit surface area (BET) of the two samples are plotted as a function of CO_2 pressure. Comparing Figure 5b and Figure 5a shows that the CO_2 uptake per surface area (BET) of the ED-ZIF-8 is obviously higher than that of the ZIF-8, which is mainly ascribed to the introduction of N—H groups, as shown in Figure 3.

Figure 6a and 6b show the N_2 adsorption isotherms on the two samples. It is visible that the N_2 uptakes on the modified ZIF-8 samples are slightly higher than that on the ZIF-8 due to its larger surface area and pore volume after modification. However, after Figure 6a and 6b are converted into Figure 7a and 7b in which the equilibrium uptakes of N_2 based on unit surface area of the two samples are plotted as a function of pressure, it is found from Figure 7 that the equilibrium uptakes of N_2 per surface area of the ED-ZIF-8 are slightly lower than that of the ZIF-8, which means that ED-ZIF-8 sample has less affinity toward N_2 than ZIF-8 sample. This will be helpful to enhance the adsorption selectivity for CO_2/N_2.

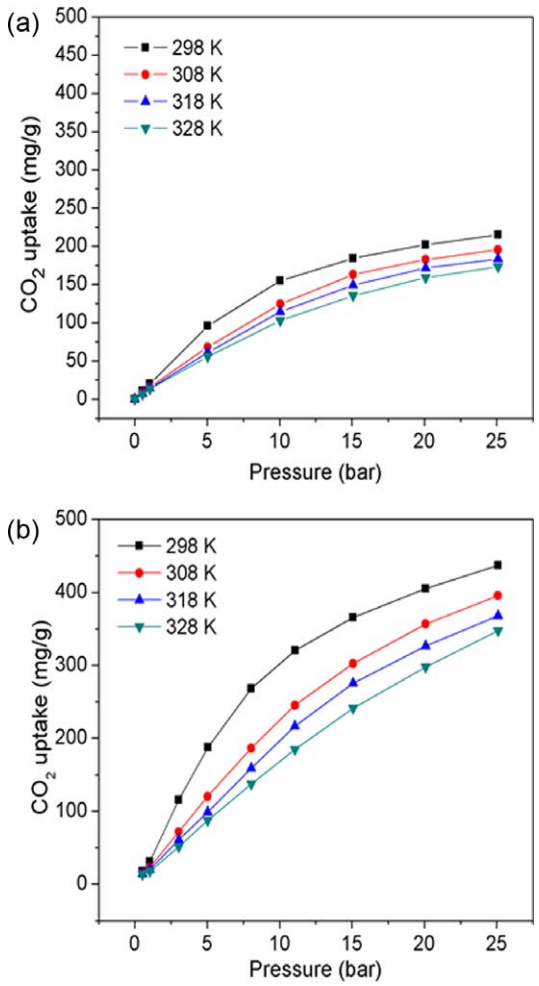

Figure 4. a. Isotherms of CO_2 on the ZIF-8 sample with different temperatures; b. isotherms of CO_2 on the ED-ZIF-8 sample with different temperatures.

[Color figure can be viewed in the online issue, which is available at wileyonlinelibrary.com.]

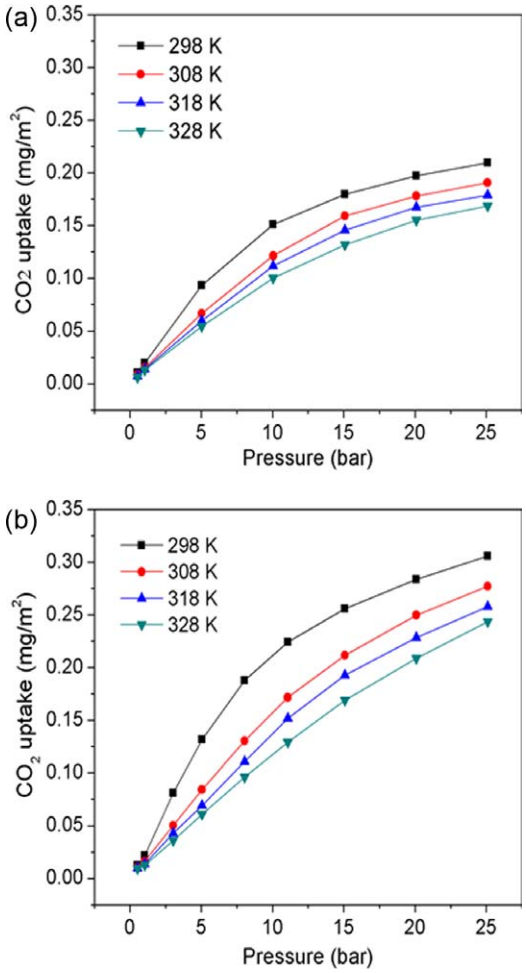

Figure 5. a. Isotherms of CO_2 on the ZIF-8 sample based on unit surface area; b. isotherms of CO_2 on the ED-ZIF-8 sample based on unit surface area.

[Color figure can be viewed in the online issue, which is available at wileyonlinelibrary.com.]

Multiple cycles of CO_2 adsorption-desorption on the ED-ZIF-8

To evaluate the regeneration performance of the modified sample or the reversibility of CO_2 adsorption on the modified sample, the experiments of multiple cycles of CO_2 adsorption-desorption on the ED-ZIF-8 were performed in the Rubotherm system at 298 K. For adsorption process, the adsorption pressure were targeted for 25 bar; while for desorption process the system pressure was targeted for 1 mbar, and then the desorption system was quickly depressurized by using vacuum pumping. Figure 8 shows the variation curve of the amounts adsorbed of CO_2 on the ED-ZIF-8 during four consecutive cycles of CO_2 adsorption-desorption experiments at 298 K. It was visible clearly that during the desorption, the amounts adsorbed of CO_2 on the ED-ZIF-8 sample decreased sharply with time, and then reached a very low content, about 2.21 wt % of residual CO_2 which was present on the sample after desorption at 1 mbar. The efficiency of CO_2 desorption was nearly up to 98% over the entire four circles. It indicated further that CO_2 adsorption was reversible with very little accumulation of irreversible bound CO_2 on the ED-ZIF-8 framework. In addition, it was also observed from Figure 8 that the curves representing the cycles of CO_2 adsorption-desorption experiments were very similar, suggesting that adsorption and desorption properties of the sample ED-ZIF-8 for CO_2 were stable or repeatable. It also proved that the pressure swing was effective in stripping adsorbed CO_2 from the ED-ZIF-8.

H_2O adsorption isotherms

Figure 9 shows the water isotherms on the modified ZIF-8 samples at 298 K. The water uptake on the ED-ZIF-8 sample is less than that on the ZIF-8 sample, indicating that the surface of the modified sample became more hydrophobic compared to the ZIF-8 sample. It also means that the interaction of the water molecule with the modified sample became weaker as compared to that with the ZIF-8.

Ideal adsorbed solution theory (IAST) selectivity of CO_2/N_2

The ideal adsorbed solution theory (IAST) developed by Myers and Praunitz[66] provides an effective method to predict the adsorption selectivity and the adsorption equilibrium of gas mixtures from the isotherms of the pure components.

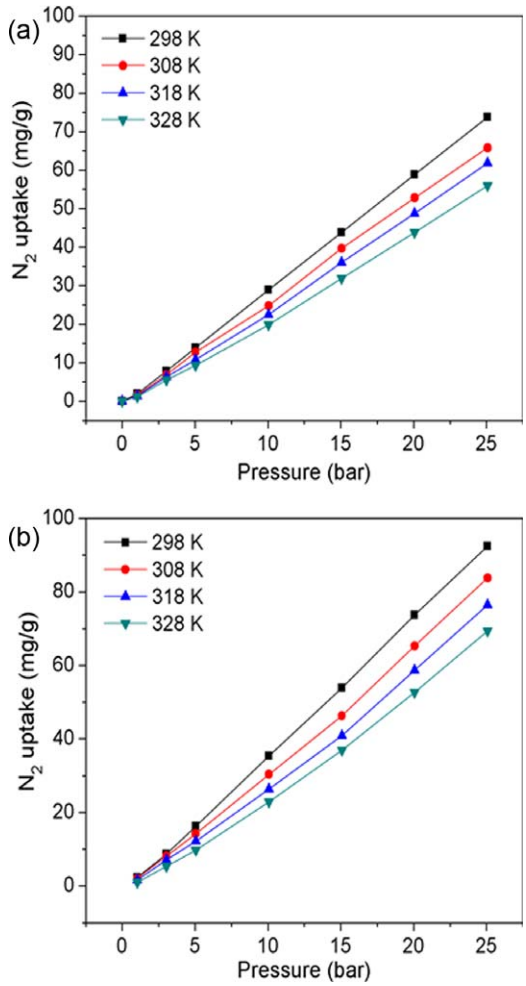

Figure 6. a. Isotherms of N_2 on the ZIF-8 sample at different temperatures; b. isotherms of N_2 on the ED-ZIF-8 sample at different temperatures.

[Color figure can be viewed in the online issue, which is available at wileyonlinelibrary.com.]

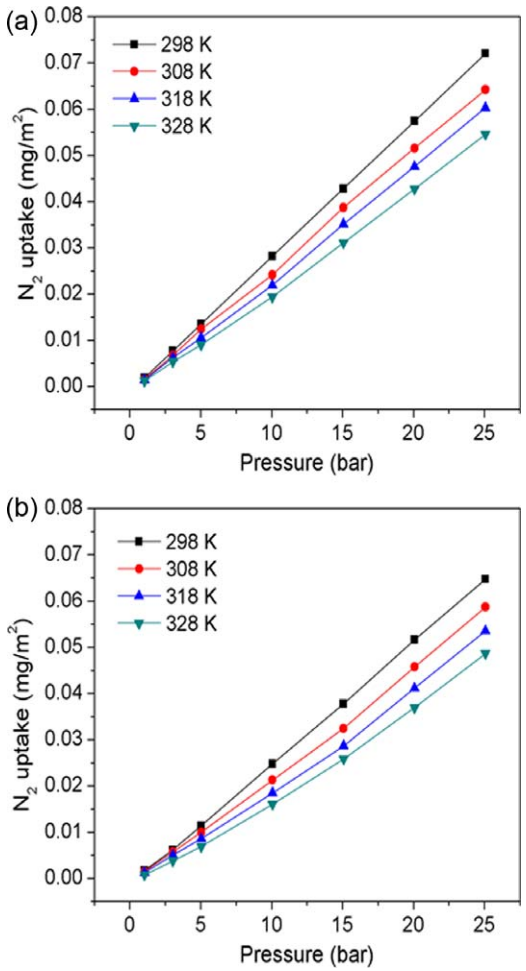

Figure 7. a. Isotherms of N_2 on the ZIF-8 sample based on unit surface area; b. isotherms of N_2 on the ED-ZIF-8 sample based on unit surface area.

[Color figure can be viewed in the online issue, which is available at wileyonlinelibrary.com.]

Previous work reported that the IAST can accurately predict gas mixture adsorption in a number of zeolites and MOF materials.[10,48,67–70]

The IAST assumes that the adsorbed mixture is an ideal solution at constant spreading pressure and temperature, where all the components in the mixture conform to the rule analogous to Raoult's law, and the chemical potential of the adsorbed solution is considered equal to that of the gas phase at equilibrium.

From the IAST, the spreading pressure π is given by

$$\pi_i^0(p_i^0) = \frac{RT}{A}\int_0^{p_i^0} q d\ln p \tag{1}$$

$$\pi^* = \frac{\pi A}{RT} = \int_0^{p_i^0} \frac{q_i}{p} dp \tag{2}$$

Where A is the specific surface area of the adsorbent, π and π^* are the spreading pressure and the reduced spreading pressure, separately. p_i^0 is the gas pressure of component i corresponding to the spreading pressure π of the gas mixture.

At a constant temperature, the spreading pressure of single component is the same

$$\pi_1^* = \pi_2^* = \ldots = \pi_n^* = \pi \tag{3}$$

For binary adsorption of component 1 and 2, the IAST requires

$$\begin{aligned} y_1 p_t &= x_1 p_1 \\ (1-y_1)p_t &= (1-x_1)p_2 \end{aligned} \tag{4}$$

Where y_1 and x_1 denote the molar fractions of component 1 in the gas phase and in the adsorbed phase, respectively. p_t is the total gas pressure, p_1 and p_2 are the pressures of component 1 and 2 at the same spreading pressure as that of the mixture, respectively.

Adsorption selectivity in a binary mixture of component 1 and 2 is defined as

$$S_{12} = \left(\frac{x_1}{x_2}\right)\left(\frac{y_2}{y_1}\right) \tag{5}$$

For the application of IAST to predict adsorption separation selectivity, the following two conditions are necessary: good quality adsorption data of each single component; and excellent curve fitting model for such data.[48,71,72]

In order to perform the integrations of Eqs. (1) and (2) required by IAST, the single-component isotherms should be fitted by a proper isotherm model. In practice, several methods are available. In this work, it is found that the dual-site Langmuir-Freundlich (DSLF) equation can be successful to fit this set of adsorption data. The dual-site Langmuir-Freundlich model can be expressed as follows

$$q = q_{m,1}\times\frac{b_1 p^{1/n_1}}{1+b_1 p^{1/n_1}} + q_{m,2}\times\frac{b_2 p^{1/n_2}}{1+b_2 p^{1/n_2}} \tag{6}$$

Where p is the pressure of the bulk gas at equilibrium with the adsorbed phase (kPa), $q_{m,1}$, $q_{m,2}$ are the saturation capacities of sites 1 and 2 (mmol/g), b_1 and b_2 are the affinity coefficients of sites 1 and 2 (1/kPa), and n_1 and n_2 are the deviations from an ideal homogeneous surface.

Figure 10 shows a comparison of the model fits and the isotherm data. It is visible that the DSLF model can be applied favorably for fitting experimental data of CO_2 and N_2 adsorption. Table 2 presents the fitting parameters of

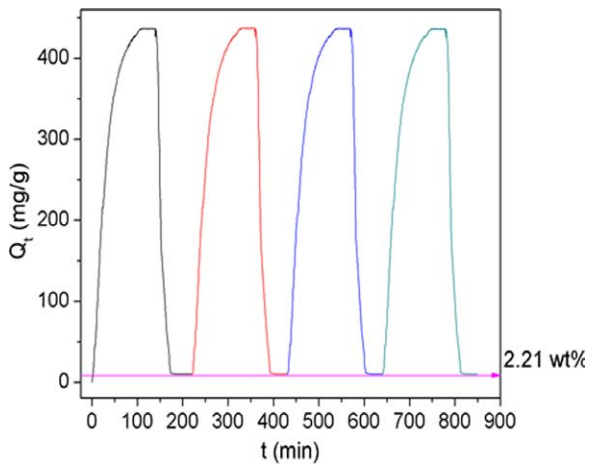

Figure 8. Recycle runs of CO_2 adsorption-desorption on the ED-ZIF-8 at 298 K and 25 bar for adsorption and 1 mbar for desorption.

[Color figure can be viewed in the online issue, which is available at wileyonlinelibrary.com.]

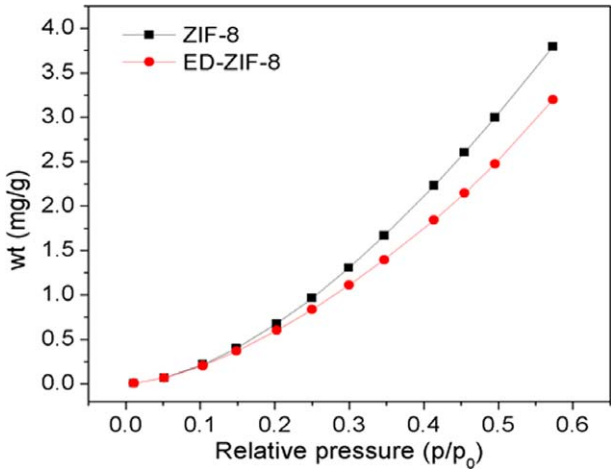

Figure 9. H_2O adsorption isotherms on the modified ZIF-8 samples at 298 K.

[Color figure can be viewed in the online issue, which is available at wileyonlinelibrary.com.]

DSLF equation as well as the correlation coefficients (R^2). Examination of the data shows that this DSLF model is able to fit the adsorption data well since the correlation coefficients R^2 are up to 0.9997.

In this work, the equilibrium adsorption data of single component CO_2 as well as N_2 are available, and the DSLF model can fit the experimental isotherms of CO_2 and N_2 adsorption very well. Therefore, the DSLF model can be combined with the ideal adsorbed solution theory (IAST) to predict the mixture adsorption isotherms and calculate the selectivities of the two samples for CO_2/N_2 adsorption.

Figure 11a and 11b present, respectively, the adsorption isotherms predicted by IAST for equimolar mixtures of CO_2/N_2 in the samples ZIF-8 and ED-ZIF-8 as a function of total bulk pressure. It can be seen that CO_2 is preferentially adsorbed over N_2 on the two samples because of stronger interactions between CO_2 and the ZIF-8 sample, and the amount adsorbed of N_2 is much lower in the mixtures than that in single-component adsorption because of competition adsorption from CO_2, which adsorbs more strongly.

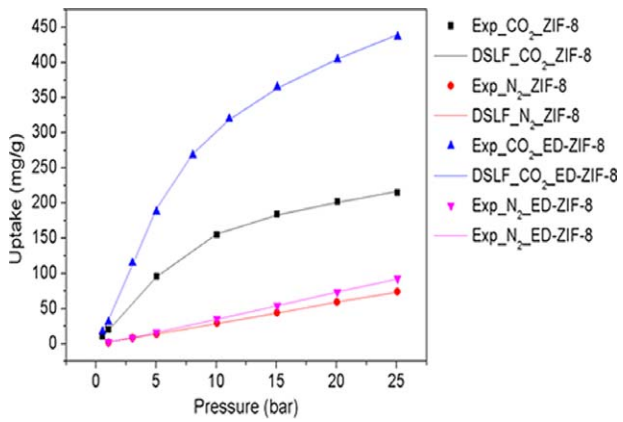

Figure 10. DSLF fitting of the CO_2 and N_2 isotherms on ZIF-8 and ED-ZIF-8 at 298 K.

[Color figure can be viewed in the online issue, which is available at wileyonlinelibrary.com.]

Table 2. The Fitting Parameters of the Dual-site Langmuir-Freundlich Equations for the Pure Isotherms of CO_2 and N_2 at 298 K

	ZIF-8		ED-ZIF-8	
	CO_2	N_2	CO_2	N_2
R^2	0.9997	0.9999	0.9997	0.9999
$q_{m,1}$ (mmol/g)	27.25	27.87	48.88	28.32
$q_{m,2}$ (mmol/g)	2.122	1.919	4.672	1.847
b_1 (atm^{-1})	0.01533	0.001170	0.01259	0.001388
b_2 (atm^{-1})	0.006895	0.02609	0.02948	0.02504
n_1	1.600	0.7875	1.404	0.7704
n_2	0.3244	0.9634	0.4430	0.8671

Figure 12 shows the IAST-predicted selectivities of the two samples for equimolar CO_2 and N_2 mixtures at 298 K as a function of total bulk pressure. It can be seen that the adsorption selectivity of the two samples for CO_2/N_2 dropped with an increase in the pressure. More importantly,

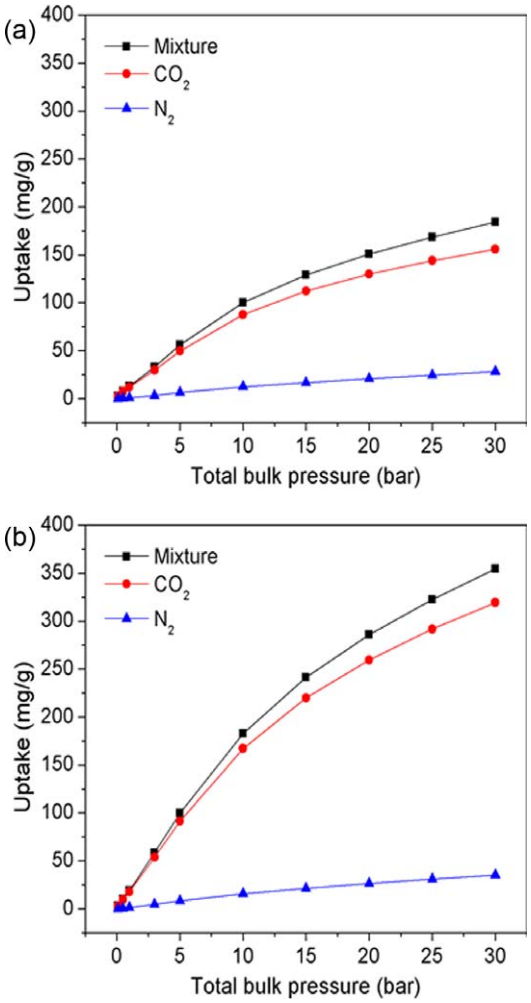

Figure 11. a. The IAST-predicted isotherm for equimolar CO_2/N_2 mixtures of the ZIF-8 sample at 298 K as a function of total bulk pressure; b. the IAST-predicted isotherm for equimolar CO_2/N_2 mixtures of the ED-ZIF-8 sample at 298 K as a function of total bulk pressure.

[Color figure can be viewed in the online issue, which is available at wileyonlinelibrary.com.]

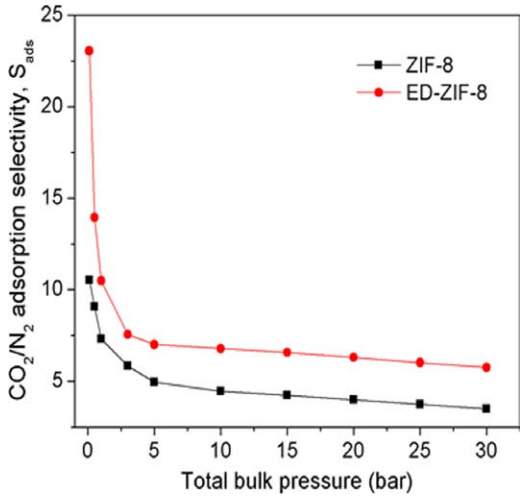

Figure 12. The IAST-predicted selectivity for equimolar CO_2 and N_2 at 298 K as a function of total bulk pressure.

[Color figure can be viewed in the online issue, which is available at wileyonlinelibrary.com.]

the adsorption selectivity of CO_2/N_2 on the sample ED-ZIF-8 is always higher than that on the sample ZIF-8, especially in the low-pressure region. For example, at 0.1 and 0.5 bar, the selectivity of the sample ED-ZIF-8 for CO_2/N_2 were up to 23 and 13.9 separately, which is almost twice of those of the sample ZIF-8.

Figure 13a and 13b show, respectively, the IAST-predicted selectivities of the samples ZIF-8 and ED-ZIF-8 for CO_2/N_2 at different mixture compositions and different pressures. It is noticed that the selectivity increases rapidly as the gas-phase mole fraction of N_2 approaches unity. For example, at $yN_2 = 0.9$, a typical feed composition of flue gas, high selectivities are obtained. Even at $yN_2 = 0.5$, the selectivity of the ED-ZIF-8 for CO_2/N_2 is in the range of 6–24, much higher than those on the ZIF-8 sample and many other MOF samples such as ZIF-70[30], ZIF-68[30] and MOF-508b.[73] This property is very important since some separation processes could be operated at low pressures, such as vacuum swing adsorption (VSA), which could be extremely efficient by using the sample ED-ZIF-8 because its selectivity increases dramatically with decreasing pressure.

Ideal adsorbed solution theory (IAST) selectivity of $CO_2/N_2/H_2O$

The major challenge of CO_2 capture from power plant flue gas wastes is the separation of CO_2/N_2. In addition, competition adsorption of water molecule must be taken into account, because these flue gas wastes are usually saturated with certain amount of water (5–7% by volume) for the industrial postcombustion processes. Thus, for real industrial use of adsorbents, the effect of water on CO_2/N_2 selectivity is another crucial factor that needs to be considered and evaluated. Here, the IAST was adopted to evaluate the ternary mixture $CO_2/N_2/H_2O$ adsorption on the modified ZIF-8 samples.

First, the experimental isotherms of water on the modified ZIF-8 samples at 298 K were fitted using the DSLF model. Table 3 presents the fitting parameters of DSLF equation as well as the correlation coefficients. It can be seen that the DSLF model fits the H_2O adsorption on both samples very well. Second, the DSLF model was combined with the ideal adsorbed solution theory (IAST) to predict the mixture adsorption isotherms, and then calculate the selectivities of the two samples for CO_2/N_2 adsorption.

Figure 14 shows the predicted isotherms of ternary mixture $CO_2/N_2/H_2O$ on the modified ZIF-8 samples at 298 K. It can be observed that in comparison with the ZIF-8, after modification, the CO_2 adsorption capacity of the ED-ZIF-8 in the ternary mixture obviously increased, and its N_2 adsorption capacity somewhat increased, which made CO_2/N_2 adsorption selectivity of the ED-ZIF-8 increase. More importantly, its water adsorption capacity in the ternary mixture became lower compared to the ZIF-8, and it was also lower than the single component water uptake. It means the competition adsorption of H_2O in the ternary mixture was weakened on the surfaces of the ED-ZIF-8 sample.

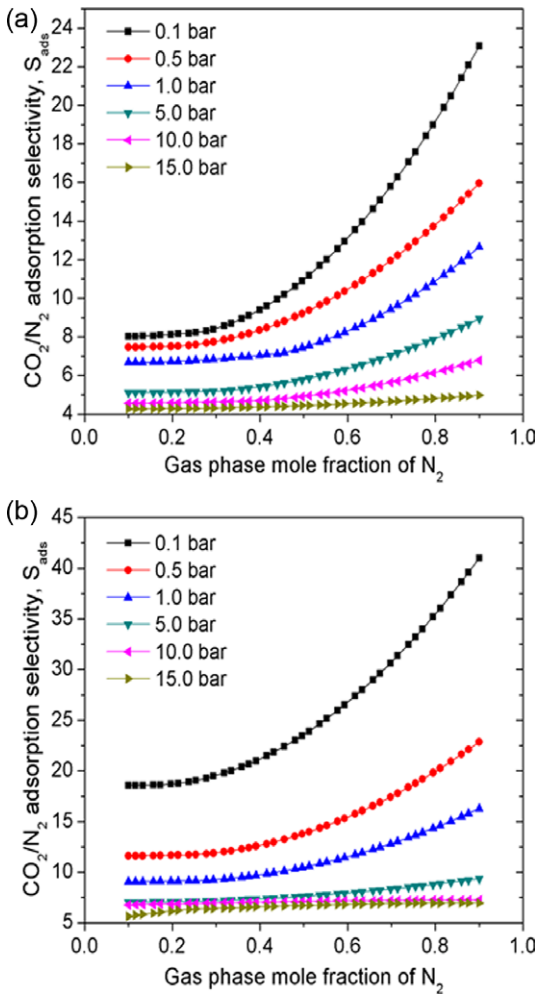

Figure 13. a. The IAST predicted selectivities at different mixture compositions and different pressures for the ZIF-8 sample at 298 K; b. the IAST predicted selectivities at different mixture compositions and different pressures for the ED-ZIF-8 sample at 298 K.

[Color figure can be viewed in the online issue, which is available at wileyonlinelibrary.com.]

Table 3. The Fitting Parameters of DSLF Equation for H_2O Adsorption on the Modified ZIF-8 Samples

Materials	$q_{m,1}$ (mmol/g)	$q_{m,2}$ (mmol/g)	b_1 (atm^{-1})	b_2 (atm^{-1})	n_1	n_2	R^2
ZIF-8	3.093	0.454	0.3893	2.117	0.1377	0.5053	0.9995
ED-ZIF-8	1.250	0.658	0.3647	0.9058	0.6170	0.1562	0.9995

Isosteric heats of adsorption

The regeneration temperature of a CO_2 capture material in a PSA or TSA process largely depends on the thermodynamics of adsorption, which is commonly expressed as the isosteric heat of adsorption *Qst*. The average interactions of adsorbent-adsorbate at a specific surface coverage are calculated by fitting isotherms at two or three temperatures with the virial[74–76] method. Here, a virial-type expression comprising the temperature-independent parameters a_i and b_i are employed to calculate the enthalpies of adsorption for CO_2 (at 298 K, 308 K, 318 K and 328 K) on the samples ZIF-8 and ED-ZIF-8. In each case, the data are fitted by using the equation

$$\ln P = \ln N + \frac{1}{T}\sum_{i=0}^{m} a_i N^i + \sum_{i=0}^{n} b_i N^i \tag{7}$$

where P is the pressure expressed in atm, N is the amount adsorbed in mg/g, T is the temperature in K, a_i and b_i are virial coefficients, and m and n represent the number of coefficients required to adequately describe the isotherms (m and n are gradually increased until the contribution of extra added a and b coefficients are deemed to be statistically insignificant toward the overall fit, and the average value of the squared deviations from the experimental values is minimized). The values of the virial coefficients a_0 through a_m are then used to calculate the isosteric heat of adsorption by using the following expression

$$Q_{st} = -R\sum_{i=0}^{m} a_i N^i \tag{8}$$

Figure 15 shows the isosteric heats of adsorption (Q_{st}) of CO_2 as a function of the amounts adsorbed of CO_2 on the two samples ZIF-8 and ED-ZIF-8, respectively. It is visible that at the onset of adsorption, Q_{st} of CO_2 adsorption on the sample ED-ZIF-8 is higher than that on the sample ZIF-8, indicating a much stronger interaction between CO_2 and the ED-ZIF-8 framework. This high Q_{st} is due to favorable interactions between adsorbed CO_2 molecules and the Lewis basic amine decorating the frameworks. In addition, the Q_{st} of CO_2 decreases with the increase in the CO_2 uptake on the ED-ZIF-8 sample. This decreasing trend of the isosteric heat of adsorption with an increase in the amount adsorbed of CO_2 can be ascribed to the surface heterogeneity of the

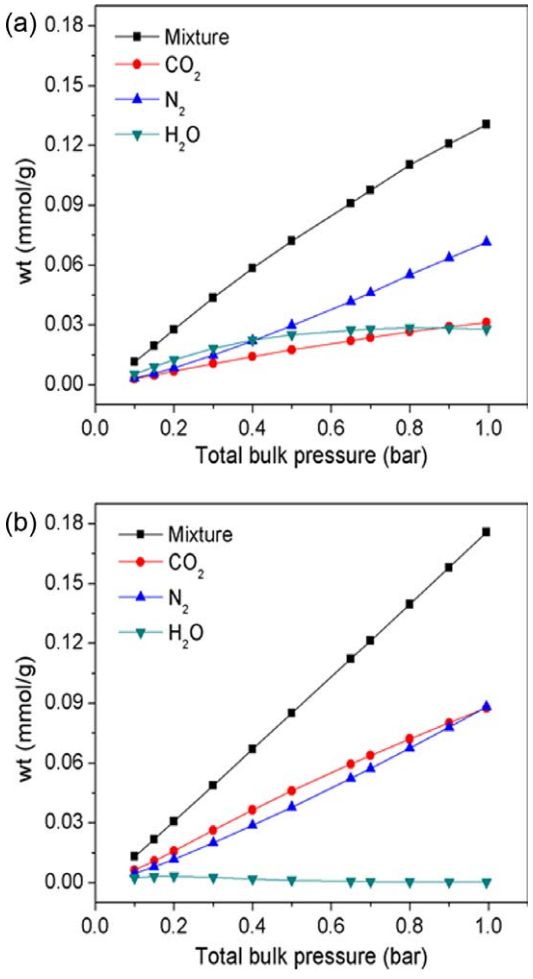

Figure 14. a. The IAST-predicted isotherm for $CO_2/N_2/H_2O$ mixtures on the ZIF-8 sample at 298 K as a function of total bulk pressure (CO_2:N_2:H_2O = 15:75:10); b. the IAST-predicted isotherm for $CO_2/N_2/H_2O$ mixtures on the ED-ZIF-8 sample at 298 K as a function of total bulk pressure (CO_2:N_2:H_2O = 15:75:10).

[Color figure can be viewed in the online issue, which is available at wileyonlinelibrary.com.]

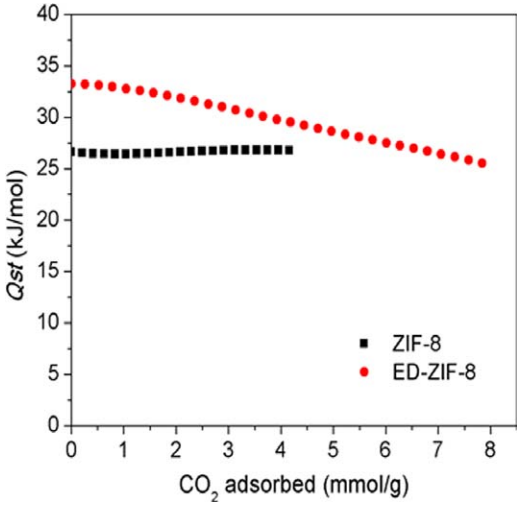

Figure 15. Dependence of isosteric heat of adsorption on the amounts adsorbed of CO_2 over the modified ZIF-8 samples.

[Color figure can be viewed in the online issue, which is available at wileyonlinelibrary.com.]

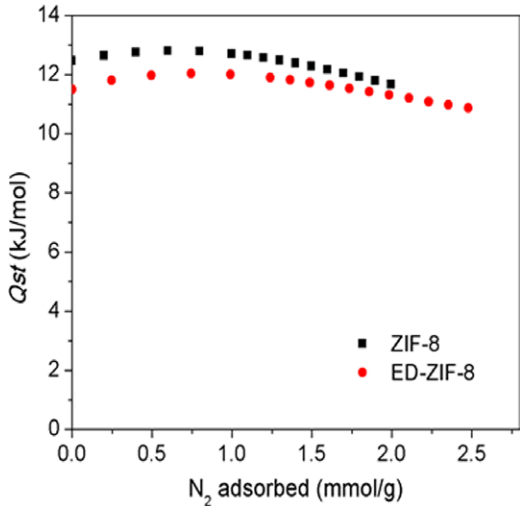

Figure 16. Dependence of isosteric heat of adsorption on the amounts adsorbed of N_2 over the modified ZIF-8 samples.

[Color figure can be viewed in the online issue, which is available at wileyonlinelibrary.com.]

ED-ZIF-8 sample. At the same time, it is noticed that Q_{st} of CO_2 on the ZIF-8 sample is nearly independent of the CO_2 loading, which means that there is no specific interaction between CO_2 molecule and the homogeneous surface of the ZIF-8 sample. Figure 16 shows that Q_{st} of N_2 adsorption as a function of the amounts adsorbed of N_2 on the two samples. A comparison of Figures 15 and 16 shows that Q_{st} of N_2 adsorption are lower than the Q_{st} of CO_2 adsorption on each of the samples, which further confirmed the favorable selectivity of the original and modified ZIF-8 samples for CO_2/N_2. Furthermore, it is interesting to point out that after modification; the Q_{st} of CO_2 adsorption on the sample ED-ZIF-8 becomes higher, while the Q_{st} of N_2 adsorption gets smaller in comparison with those on the sample ZIF-8. As a result of that, the adsorption selectivity of the ED-ZIF-8 becomes higher compared to the ZIF-8, as shown in Figure 12.

Conclusions

From foregoing discussion, following conclusions can be drawn. The ZIF-8 sample can be modified with ethylenediamine by using postsynthetic method to enhance its adsorption performance toward CO_2. The BET surface area of the modified sample (ED-ZIF-8) increases by 39% as compared to the original ZIF-8 sample, and some N—H groups are introduced on the surfaces of the ED-ZIF-8. Furthermore, the ED-ZIF-8 sample has higher CO_2 adsorption capacities compared to the ZIF-8 sample, nearly being twice as much as the ZIF-8. This increase is mainly ascribed to its larger surface area and the introduction of some N—H groups on the surface of the ED-ZIF-8. The DSLF model can be applied favorably for fitting experimental isotherm data of CO_2 and N_2 adsorption. The IAST can be applied to predict the adsorption selectivity from the pure component isotherms. The modified sample ED-ZIF-8 has higher adsorption selectivity of CO_2/N_2 than the original ZIF-8, especially in the low-pressure region. At 0.1 and 0.5 bars, the selectivities of the sample ED-ZIF-8 for CO_2/N_2 were up to 23 and 13.9, respectively, which is almost twice of those of the sample ZIF-8 at 298 K with equimolar CO_2 and N_2 mixtures. More interestingly, the uptake of water on the ED-ZIF-8 sample is less than that on the ZIF-8 sample, indicating that the surfaces of the ED-ZIF-8 became more hydrophobic compared to the ZIF-8, and that the interaction of the water molecule with the modified sample became weaker as compared to that with the ZIF-8. The predicted isotherms of ternary mixture $CO_2/N_2/H_2O$ on the ED-ZIF-8 sample exhibits that the CO_2 is more favorably adsorbed than the N_2 and H_2O molecules. The isosteric heat Q_{st} of CO_2 on the sample ED-ZIF-8 is obviously higher than that on the sample ZIF-8, while Q_{st} of N_2 is slightly lower than that on the sample ZIF-8. On the other hand, it indicates a much stronger interaction between CO_2 and the ED-ZIF-8 sample. On the other hand, the interaction between N_2 and the ED-ZIF-8 sample is weakened. It suggests that the use of postsynthetic method to modify the ZIF-8 not only improves its adsorption capacity toward CO_2, but also enhances its adsorption selectivity for CO_2/N_2.

Acknowledgments

This work was supported by National Natural Science Foundation of China (No. 20936001, 21176085). The authors greatly acknowledge the financial support by National Science Fund for Distinguished Young Scholars of China (No. 21225625). Author Z. Zhang thanks to the China Scholarship Council (CSC, 2010615043) for a fellowship to support her stay at Rutgers University, and is also grateful to the valuable discussions with Prof Katsumi Kaneko in Chiba University.

Notation

b_1, b_2 = dual-site Langmuir-Freundlich constant for species 1 and 2, atm^{-1}
n_1, n_2 = exponent of species 1 and 2 in the dual-site Langmuir-Freundlich isotherm, dimensonless
P = equilibrium pressure of the adsorbate in gas phase, bar
p_i^0 = pressure of component i that corresponding to the spreading pressure π of the gas mixture
p_1, p_2 = the pressures of component 1 and 2 at the same spreading pressure as that of the mixture
p_t = the total gas pressure
$q_{m,1}, q_{m,2}$ = saturation loading of species 1 and 2, mmol/g
S_{12} = IAST adsorption selectivity
x_1 = molar fractions of component 1 in the adsorbed phase
y_1 = molar fractions of component 1 in the gas phase

Greek letters

π = spreading pressure
π^* = reduced spreading pressure

Literature Cited

1. Lackner KS. A guide to CO_2 sequestration. *Science*. 2003;300:1677–1678.
2. Haszeldine RS. Carbon capture and storage: How green can black be? *Science*. 2009;325:1647–1652.
3. Kevitiyala N. Carbon sequestration. *Science*. 2009;325:1644–1645.
4. Firoozabadi A, Cheng P. Prospects for subsurface CO_2 sequestration. *AIChE J*. 2010;56:1398–1405.
5. Peng X, Wang W, Xue R, Shen Z. Adsorption separation of CH_4/CO_2 on mesocarbon microbeads: Experiment and modeling. *AIChE J*. 2006;52:994–1003.
6. Yang RT. Gas separation by adsorption processes. Boston, MA: Butterworths; 1987.
7. Konduru N, Lindner P, Assaf-Anid NM. Curbing the greenhouse effect by carbon dioxide adsorption with zeolite 13X. *AIChE J*. 2007;53:3137–3143.

8. Zhang Z, Zhang W, Chen X, Xia Q, Li Z. Adsorption of CO_2 on zeolite 13x and activated carbon with higher surface area. *Sep Sci Tech*. 2010;45:710–719.
9. Zhang Z, Xu M, Wang H, Li Z. Enhancement of CO_2 adsorption on high surface area activated carbon modified by N_2, H_2 and ammonia. *Chem Eng J*. 2010;160:571–577.
10. Babarao R, Hu Z, Jiang J, Chempath S, Sandler SI. Storage and Separation of CO_2 and CH_4 in Silicalite, C168 Schwarzite, and IRMOF-1: A comparative study from monte carlo simulation. *Langmuir*. 2006;23:659–666.
11. Monazam ER, Shadle LJ, Siriwardane R. Equilibrium and absorption kinetics of carbon dioxide by solid supported amine sorbent. *AIChE J*. 2011;57:3153–3159.
12. Shao X, Feng Z, Xue R et al. Adsorption of CO_2, CH_4, CO_2/N_2 and CO_2/CH_4 in novel activated carbon beads: Preparation, measurements and simulation. *AIChE J*. 2011;57:3042–3051.
13. Zhen-shan L, Ning-sheng C, Croiset E. Process analysis of CO_2 capture from flue gas using carbonation/calcination cycles. *AIChE J*. 2008;54:1912–1925.
14. Wang L, Yang RT. Increasing Selective CO_2 Adsorption on Amine-Grafted SBA-15 by Increasing Silanol Density. *J Phys Chem C*. 2011;115:21264–21272.
15. Yang Q, Xue C, Zhong C, Chen J-F. Molecular simulation of separation of CO_2 from flue gases in CU-BTC metal-organic framework. *AIChE J*. 2007;53:2832–2840.
16. Bourrelly S, Llewellyn PL, Serre C, Millange F, Loiseau T, Férey G. Different adsorption behaviors of methane and carbon dioxide in the isotypic nanoporous metal terephthalates MIL-53 and MIL-47. *J Am Chem Soc*. 2005;127:13519–13521.
17. Eddaoudi M, Kim J, Rosi N, Vodak D, Wachter J, O'Keeffe M, Yaghi OM. Systematic design of pore size and functionality in isoreticular mofs and their application in methane storage. *Science*. 2002;295:469–472.
18. Millward AR, Yaghi OM. Metal organic frameworks with exceptionaly high capacity for storage of carbon dioxide at room temperature. *J Am Chem Soc*. 2005;127:17998–17999.
19. Furukawa H, Yaghi OM. Storage of hydrogen, methane, and carbon dioxide in highly porous covalent organic frameworks for clean energy applications. *J Am Chem Soc*. 2009;131:8875–8883.
20. Zhang Z, Huang S, Xian S, Xi H, Li Z. Adsorption equilibrium and kinetics of CO_2 on chromium terephthalate MIL-101. *Energy Fuels*. 2011;25:835–842.
21. Li J-R, Ma Y, McCarthy MC et al. Carbon dioxide capture-related gas adsorption and separation in metal-organic frameworks. *Coord Chem Rev*. 2011;255:1791–1823.
22. Zhang J, Wu H, Emge TJ, Li J. A flexible MMOF exhibiting high selectivity for CO_2 over N_2, CH_4 and other small gases. *Chem Commmun*. 2010;46:9152–9154.
23. Wu H, Reali RS, Smith DA, Trachtenberg MC, Li J. Highly Selective CO_2 capture by a flexible microporous metal-organic framework (mmof) material. *Chem Eur J*. 2010;16:13951–13954.
24. Zhao Y, Wu H, Emge TJ et al. Enhancing gas adsorption and separation capacity through ligand functionalization of microporous metal-organic framework structures. *Chem Eur J*. 2011;17:5101–5109.
25. Gassensmith JJ, Furukawa H, Smaldone RA et al. Strong and reversible binding of carbon dioxide in a green metal-organic framework. *J Am Chem Soc*. 2011;133:15312–15315.
26. Samanta A, Zhao A, Shimizu GKH, Sarkar P, Gupta R. Post-combustion CO_2 capture using solid sorbents: A review. *Ind Eng Chem Res*. 2011;51:1438–1463.
27. Builes S, Roussel T, Ghimbeu CM et al. Microporous carbon adsorbents with high CO_2 capacities for industrial applications. *Phys Chem Chem Phys*. 2011;13:16063–16070.
28. Liu H, Zhao Y, Zhang Z, Nijem N, Chabal YJ, Zeng H, Li J. The effect of methyl functionalization on microporous metal-organic frameworks' capacity and binding energy for carbon dioxide adsorption. *Adv Func Mater*. 2011;21:4754–4762.
29. Phan A, Doonan CJ, Uribe-Romo FJ, Knobler CB, O'Keeffe M, Yaghi OM. Synthesis, structure, and carbon dioxide capture properties of zeolitic imidazolate frameworks. *Acc Chem Res*. 2009;43:58–67.
30. Banerjee R, Furukawa H, Britt D, Knobler C, O'Keeffe M, Yaghi OM. Control of pore size and functionality in isoreticular zeolitic imidazolate frameworks and their carbon dioxide selective capture properties. *J Am Chem Soc*. 2009;131:3875–3877.
31. Morris W, Leung B, Furukawa H, Yaghi OK, He N, Hayashi H, Houndonougbo Y, Asta M, Laird BB, Yaghi OM. A combined experimental–computational investigation of carbon dioxide capture in a series of isoreticular zeolitic imidazolate frameworks. *J Am Chem Soc*. 2010;132:11006–11008.
32. An J, Geib SJ, Rosi NL. High and Selective CO_2 uptake in a cobalt adeninate metal–organic framework exhibiting pyrimidine- and amino-decorated pores. *J Am Chem Soc*. 2009;132:38–39.
33. An J, Rosi NL. Tuning MOF CO_2 adsorption properties via cation exchange. *J Am Chem Soc*. 2010;132:5578–5579.
34. Couck S, Denayer JFM, Baron GV, Rémy T, Gascon J, Kapteijn F. An amine-functionalized mil-53 metal–organic framework with large separation power for CO_2 and CH_4. *J Am Chem Soc*. 2009;131:6326–6327.
35. Arstad B, Fjellvag H, Kongshaug KO, Swang O, Blom R. Amine functionalised metal organic frameworks (MOFs) as adsorbents for carbon dioxide. *Adsorption*. 2008;14:755–762.
36. Vaidhyanathan R, Iremonger SS, Dawson KW, Shimizu GKH. An amine-functionalized metal organic framework for preferential CO_2 adsorption at low pressures. *Chem Commmun*. 2009:5230–5232.
37. Vaidhyanathan R, Iremonger SS, Shimizu GKH, Boyd PG, Alavi S, Woo TK. Direct observation and quantification of CO_2 binding within an amine-functionalized nanoporous solid. *Science*. 2010;330:650–653.
38. Vaidhyanathan R, Iremonger SS, Shimizu GKH, Boyd PG, Alavi S, Woo TK. Competition and cooperativity in carbon dioxide sorption by amine-functionalized metal-organic frameworks. *Angew Chem Int Ed*. 2012;51:1826–1829.
39. Li B, Zhang Z, Li Y et al. Enhanced binding affinity, remarkable selectivity, and high capacity of CO_2 by dual functionalization of a rht-type metal-organic framework. *Angew Chem Int Ed*. 2012;51:1412–1415.
40. Farha OK, Bae Y-S, Hauser BG et al. Chemical reduction of a diimide based porous polymer for selective uptake of carbon dioxide versus methane. *Chem Commmun*. 2010;46:1056–1058.
41. Bae Y-S, Hauser BG, Farha OK, Hupp JT, Snurr RQ. Enhancement of CO_2/CH_4 selectivity in metal-organic frameworks containing lithium cations. *Micro Meso Mater*. 2011;141:231–235.
42. Babarao R, Jiang J. Unprecedentedly high selective adsorption of gas mixtures in rho zeolite-like metal–organic framework: a molecular simulation study. *J Am Chem Soc*. 2009;131:11417–11425.
43. Yoon JW, Jhung SH, Hwang YK, Humphrey SM, Wood PT, Chang JS. Gas-sorption selectivity of CUK-1: A porous coordination solid made of cobalt(ii) and pyridine-2,4- dicarboxylic acid. *Adv Mater*. 2007;19:1830–1834.
44. Dybtsev DN, Chun H, Yoon SH, Kim D, Kim K. Microporous manganese formate: a simple metal–organic porous material with high framework stability and highly selective gas sorption properties. *J Am Chem Soc*. 2003;126:32–33.
45. Loiseau T, Lecroq L, Volkringer C et al. MIL-96, a porous aluminum trimesate 3D structure constructed from a hexagonal network of 18-membered rings and μ3-Oxo-centered trinuclear units. *J Am Chem Soc*. 2006;128:10223–10230.
46. Bae Y-S, Farha OK, Hupp JT, Snurr RQ. Enhancement of CO_2/N_2 selectivity in a metal-organic framework by cavity modification. *J Mater Chem*. 2009;19:2131–2134.
47. Bae Y-S, Spokoyny AM, Farha OK, Snurr RQ, Hupp JT, Mirkin CA. Separation of gas mixtures using Co(II) carborane-based porous coordination polymers. *Chem Commmun*. 2010;46:3478–3480.
48. Bae Y-S, Farha OK, Spokoyny AM, Mirkin CA, Hupp JT, Snurr RQ. Carborane-based metal-organic frameworks as highly selective sorbents for CO_2 over methane. *Chem Commmun*. 2008:4135–4137.
49. Dietzel PDC, Besikiotis V, Blom R. Application of metal-organic frameworks with coordinatively unsaturated metal sites in storage and separation of methane and carbon dioxide. *J Mater Chem*. 2009;19:7362–7370.
50. Caskey SR, Wong-Foy AG, Matzger AJ. Dramatic tuning of carbon dioxide uptake via metal substitution in a coordination polymer with cylindrical pores. *J Am Chem Soc*. 2008;130:10870–10871.
51. Yazaydın AO, Snurr RQ, Park T-H et al. Screening of metal-organic frameworks for carbon dioxide capture from flue gas using a combined experimental and modeling approach. *J Am Chem Soc*. 2009;131:18198–18199.
52. Wang Z, Cohen SM. Postsynthetic covalent modification of a neutral metal–organic framework. *J Am Chem Soc*. 2007;129:12368–12369.
53. Wang Z, Tanabe KK, Cohen SM. Accessing postsynthetic modification in a series of metal-organic frameworks and the influence of framework topology on reactivity. *Inorg Chem*. 2008;48:296–306.

54. Tanabe KK, Cohen SM. Postsynthetic modification of metal-organic frameworks-a progress report. *Chem Soc Rev*. 2011;40:498–519.
55. Wang Z, Cohen SM. Postsynthetic modification of metal-organic frameworks. *Chem Soc Rev*. 2009;38:1315–1329.
56. An J, Geib SJ, Rosi NL. Cation-triggered drug release from a porous zinc–adeninate metal–organic framework. *J Am Chem Soc*. 2009;131:8376–8377.
57. Farha OK, Mulfort KL, Hupp JT. An example of node-based postassembly elaboration of a hydrogen-sorbing, metal-organic framework material. *Inorg Chem*. 2008;47:10223–10225.
58. Demessence A, D'Alessandro DM, Foo ML, Long JR. Strong CO_2 binding in a water-stable, triazolate-bridged metal–organic framework functionalized with ethylenediamine. *J Am Chem Soc*. 2009;131:8784–8786.
59. McDonald TM, D'Alessandro DM, Krishna R, Long JR. Enhanced carbon dioxide capture upon incorporation of N,N′-dimethylethylenediamine in the metal-organic framework CuBTTri. *Chem Sci*. 2011;2:2022–2028.
60. Zhang Z, Xian S, Xi H, Wang H, Li Z. Improvement of CO_2 adsorption on ZIF-8 crystals modified by enhancing basicity of surface. *Chem Eng Sci*. 2011;66:4878–4888.
61. Park HJ, Cheon YE, Suh MP. Post-synthetic reversible incorporation of organic linkers into porous metal-organic frameworks through single-crystal-to-single-crystal transformations and modification of gas-sorption properties. *Chem Eur J*. 2010;16:11662–11669.
62. Xiang Z, Hu Z, Cao D et al. Metal-organic frameworks with incorporated carbon nanotubes: improving carbon dioxide and methane storage capacities by lithium doping. *Angew Chem Int Ed*. 2011;50:491–494.
63. Banerjee R, Phan A, Wang B, Knobler C, Furukawa H, O'Keeffe M, Yaghi OM. High-throughput synthesis of zeolitic imidazolate frameworks and application to CO_2 capture. *Science*. 2008;319:939–943.
64. Chen B, Liang C, Yang J et al. A microporous metal-organic framework for gas-chromatographic separation of alkanes. *Angew Chem Int Ed*. 2006;45:1390–1393.
65. Reichenbach C, Kalies G, Enke D, Klank D. Cavitation and pore blocking in nanoporous glasses. *Langmuir*. 2011;27:10699–10704.
66. Myers AL, Prausnitz JM. Thermodynamics of mixed-gas adsorption. *AIChE J*. 1965;11:121–127.
67. Krishna R, Long JR. Screening metal-organic frameworks by analysis of transient breakthrough of gas mixtures in a fixed bed adsorber. *J Phys Chem C*. 2011;115:12941–12950.
68. Zhou L, Wu J, Li M, Wu Q, Zhou Y. Prediction of multicomponent adsorption equilibrium of gas mixtures including supercritical components. *Chem Eng Sci*. 2005;60:2833–2844.
69. Ryan P, Farha OK, Broadbelt LJ, Snurr RQ. Computational screening of metal-organic frameworks for xenon/krypton separation. *AIChE J*. 2011;57:1759–1766.
70. Zhang Z, Liu J, Li Z, Li J. Experimental and theoretical investigations on the MMOF selectivity for CO_2vs. N_2 in flue gas mixtures. *Dalton Trans*. 2012;41:4232–4238.
71. Bae Y-S, Mulfort KL, Frost H, Ryan P, Punnathanam S, Broadbelt LJ, Hupp JT, Snurr RQ. Separation of CO_2 from CH_4 using mixed-ligand metal–organic frameworks. *Langmuir*. 2008;24:8592–8598.
72. Belmabkhout Y, Sayari A. Adsorption of CO_2 from dry gases on MCM-41 silica at ambient temperature and high pressure. 2: Adsorption of CO_2/N_2, CO_2/CH_4 and CO_2/H_2 binary mixtures. *Chem Eng Sci*. 2009;64:3729–3735.
73. Bastin L, Barcia PS, Hurtado EJ, Silva JAC, Rodrigues AE, Chen B. A microporous metal–organic framework for separation of CO_2/N_2 and CO_2/CH_4 by fixed-bed adsorption. *J Phys Chem C*. 2008;112:1575–1581.
74. Czepirski L, Jagiello J. Virial-type thermal equation of gas-solid adsorption. *Chem Eng Sci*. 1989;44:797–801.
75. Rowsell JLC, Yaghi OM. Effects of functionalization, catenation, and variation of the metal oxide and organic linking units on the low-pressure hydrogen adsorption properties of metal–organic frameworks. *J Am Chem Soc*. 2006;128:1304–1315.
76. Britt D, Furukawa H, Wang B, Glover TG, Yaghi OM. Highly efficient separation of carbon dioxide by a metal-organic framework replete with open metal sites. *Proc Natl Acad Sci*. 2009;106:20637–20640.

Manuscript received July 24, 2012, and revision received Oct. 23, 2012.